High-Temperature Conductivity and Creep of Polycrystalline Al_2O_3 Doped with Fe and/or Ti

M. M. El-AIAT, L. D. HOU, S. K. TIKU, H. A. WANG,[*,*] and F. A. KRÖGER[*]

Department of Materials Science, University of Southern California, Los Angeles, California 90007

Partial ionic and electronic dc conductivities and compressional creep rate were measured for hot-pressed polycrystalline Al_2O_3 made from Al-isopropoxide (Al_2O_3(II)). The undoped material was found to contain 1.5×10^{18} cm^{-3} fixed valency acceptors (Mg). Properties of undoped material and material doped with Fe or Ti were investigated as a function of grain size, dopant concentration, oxygen pressure, and temperature. No fast ionic conduction along grain boundaries is found in either acceptor- or donor-dominated material. Absolute values of self-diffusion coefficients calculated from conductivity and creep indicate that both effects are limited by migration of Al, involving V_{Al}''' in donor-, $Al_i^{\cdot\cdot\cdot}$ in acceptor-dominated material. In creep, oxygen is transported along grain boundaries in a neutral form ($O_i^{\times}$). The p_{O_2} dependence of σ_i and σ_h are as expected on the basis of a defect model. That of creep is weaker for reasons that are not entirely clear. An ionic conductivity with low activation energy, observed at low temperature, is attributed to the presence of Al-silicate second phase.

I. Introduction

Alpha Al_2O_3 is an important high-temperature ceramic material and it is of considerable interest to understand the dependence of its physical properties on composition, grain size, density, oxygen pressure, and temperature. Extensive studies have been made for such properties separately, both for single crystals and for polycrystalline materials. Results are summarized in Tables I and II. Defect models explaining these results have been proposed.[12,20,36,37,39-41] Such models, if correct, should account for all the properties of a material. Unfortunately, the reliability of these models in predicting properties cannot be checked satisfactorily for results obtained with different materials: all properties

Table I. Activation Enthalpies of Processes Involving Atomic Migration

Process	Grain size (μm)	Activation enthalpy (kJ/mol)	Activation enthalpy (eV)	Remarks	Refs.
Al tracer diffusion	130–200	465	4.94		1
^{18}O diffusion	Single crystal	240	2.5	$T < 1650°C$ (dislocation mechanism)	2
		634±106	6.59±1.1	$T > 1650°C$	2
	20–30	459±62.5	4.77±0.65	$T > 1450°C$	2
	Single crystal	739	7.68	1585–1840°C, $\perp(1\bar{1}2)$	3,4
	Single crystal ± Mg or Ti	615±40	6.38±0.42		5
Neck growth	Single-crystal spheres	563	5.85	Wet H_2	6
		689	7.16	Dry H_2	6
	Single crystal spheres	689	7.16		7
Initial sintering (shrinkage)	0.3	625	6.5		8
	0.2–20	584–643	6.07–6.68	D_{gb}, D_{bulk}	9,10,11
	0.2	689	7.16		7
	5–20	625	6.5	D_{bulk}, undoped	12
	15–20	702.5	7.3	D_{bulk}, +Fe $\propto [Fe]^{0.67-0.73} p_{O_2}^{-0.3}$	
Intermediate and final-stage sintering	0.3	625	6.5		13
Creep	18	284±115	2.95±1.2		14
	3–30	543	5.64		15,16
	30–100	689	7.16	Dislocation climb	16
	10	567	5.90	$T < 1800°C$	17
	Single crystal	750	7.8	Dislocation climb	18
	Single crystal	828	8.6	Dislocation climb	19
	26–75	924	9.6	$T > 1800°C$	19
	3–42	475	4.94	+Cr	20
		611±6	6.35±0.06	+Fe; $\propto p_{O_2}^{-3/16}$	20
		711	8.02	+Ti, $\propto p_{O_2}^{1/10}$, 2nd phase?	20
Surface scratch smoothing	Single crystal	543	5.64	$D_{surface}$	21

Received October 26, 1979; revised copy received April 14, 1980.

Supported by the U.S. Department of Energy under Contract No. EY-76-03-0113, Project Agreement 27.

[*] Member, the American Ceramic Society

[*] Now with Signetics Corp., Sunnyvale, California 94088.

Table II. Activation Enthalpies of Conductivity

Dopant	Grain size (μm)	Conditions	H (kJ/mol)	H (eV)	Type of conductivity	Refs.
None	Single crystal	Air	447	4.64		22
None	Single crystal	Air	385*	4.0*		23
None	12–20	Air, 800–1200°C	192.5*	2.0*		
		Air, $T<800$°C	86–96*	0.9-1*	σ_{gb}	
None, Co, Mg	Single crystal	Air	279*	2.9*	σ_h (?)	24
Ti	Single crystal	Air	279*	2.9*	σ_i	
Mg	20	Air	125*	1.3*	σ_h	25
		30 Pa O_2	154	1.6	Mixed	
None	Single crystal	10^5 Pa O_2	115; 145	1.2; 1.5	σ_i; σ_h	26
		10^{-3} Pa O_2	250±48	2.6±0.5	σ_i	27
None	Single crystal	800°–1100°C	96.2	1.0		
		1100°–1650°C	240[‡]	2.5		
None	Single crystal	1650°–1800°C	481	5		
None	Single crystal	850°–1500°C, 1–10^5 Pa	240	3[‡]	σ_h (?)	28
None	Single crystal	1200°–1500°C, air	270; 145	2.8; 1.5	σ_h; σ_i	29
Mg	MgO-doped Al_2O_3 tube[†]	10^5 Pa O_2	258	2.68	σ_h	30
		100 CO_2/1 CO	305	3.17	Mixed	
None	Single-crystal tube[§]	10^5 Pa O_2, $T<1400$°C	238	2.47	σ_i(?)	
		$T>1400$°C	334	3.47	σ_h	
Fe	20–900	10^5 Pa O_2	9.6; 38.5	0.1; 0.4	Hopping (?)	31
None	Single crystal tube[§]	Air	462	4.8		32
		0.8 Pa O_2	414	4.3		
	Polycrystalline tube[¶]	1200°–1500°C, 4.3 Pa O_2, air	308	3.2		
		$T<1200$°C	212	2.2		
None, Mn, Fe	Single crystal	700°–1200°C, 10^{-4} Pa O_2	124–231	1.8–2.4		33
		1300°–1550°C	385–433	4.0–4.5		
Fe	Single crystal	Air, 1000°–1600°C	481	5		34
None	Single crystal	Air, 1600°–2000°C	750	7.8		35
Co	Single crystal	10^5 Pa O_2	255*	2.65*	σ_h	36
		<10 Pa O_2	382*	3.97*	σ_i	
Fe	Single crystal	10^5 Pa O_2, $T>1625$°C	558.5	5.8	$(\sigma_i)_{eq.}$	37,38
		<1625°C	273	2.84	$(\sigma_i)_{noneq}$	
		10^5 Pa O_2	286	2.97	σ_h	
Mg	Single crystal	10^{-2}–10^{-4} Pa O_2	443–462*	4.6–4.8*	σ_i	39
		10^5 Pa O_2	195–204*	2.03–2.12*		
Ti	Single crystal	10^5 Pa O_2, eq.; noneq.	334*;363*	3.48;3.78*	(σ_i)eq.; noneq.	40
		10^{-2} Pa O_2 eq.; noneq.	306*; 322*	3.18*; 3.35*	Mixed	
Acceptor	Single crystal**	10^5 Pa O_2, eq.; noneq.	265*;337*	2.55*;3.51*	(σ_h) eq.; noneq.	41
		10^{-2} Pa O_2, eq.;	258*;363*	2.68*;377*	Mixed	
Acceptor	Single crystal[§]	10^5 Pa O_2, eq.; noneq.	445*	4.63*	σ_h	
		10^{-3} Pa O_2, eq.; noneq.	416*;455*	4.33*;4.74*	Mixed	

*Measured with elimination of surface and gas-phase conduction (dc). [†] Lucalox, General Electric Co., Schenectady, N.Y. [‡] Measured with elimination of surface and gas-phase conduction (ac and dc). [§] Tyco, Saphikon Div., Tyco Laboratories, Inc., Waltham, Mass. [¶] Morganite. **Union Carbide Corp., San Diego, Calif.

depend on the presence of impurities or dopants and, for polycrystalline material, on grain size and porosity, and these quantities as a rule differ for different samples. It is therefore necessary to study several properties on the same batch of a material.

A previous paper[42] reports on such a study, with dc conductivity and creep as the properties investigated and grain size, dopant concentration, temperature, and oxygen pressure as the variables. Grain-size variation influences the relative importance of grain boundaries which affect different properties in different ways. Creep is affected through the possibility of grain-boundary diffusion of one or both of the components. Conductivity may be either increased or decreased, depending on whether the grain boundary represents a favorable current path or acts as a barrier.[43] Even without a detailed model, it is obvious that conductivity will decrease with grain size in the former but increase in the latter case. Therefore grain-size dependence of conductivity should indicate whether appreciable grain-boundary conduction does or does not occur.

In our former study,[42] polycrystalline samples were made by hot-pressing Al_2O_3 powder made from reagent-grade aluminum sulfate, undoped and doped with iron. The undoped material proved to be acceptor-dominated, with Mg the probable acceptor impurity present at a concentration of 3×10^{18} cm^{-3}. The samples showed mixed conductivity, with conductivity dominated by ions at low, by electrons (holes) at high oxygen pressure. Grain-size dependence of the two conductivities showed indications of considerable grain-boundary conductivity by holes but not by ions.

At small grain sizes and low temperatures, creep was found to be limited by bulk diffusion (Nabarro-Herring mechanism) with activation energies of 462 to 625 kJ/mol, consistently larger than the activation energies of 327 to 423 kJ/mol found for ionic conduction. At large grain sizes and/or high temperatures, creep was independent of grain size and proportional to the square of the stress, indicating limitation by a dislocation mechanism with an activation energy of 847 kJ/mol.

A satisfactory model accounting for all the observed effects could not be found. The present paper reports on a repetition of the experiments of iron-doped Al_2O_3 as a function of grain size, p_{O_2}, and temperature in order to check the most essential results, as well as on similar experiments with Al_2O_3 doped with titanium, a

Table III. Hot-Pressing and Annealing Conditions for Al_2O_3(II) Samples Made from Distilled Aluminum Isopropoxide

Sample composition and No.	Hot-pressing temp. (°C)	Time at 55 MN/m^2 (h)	Annealing conditions temp. (°C)	Annealing conditions Time (h)	Grain size (μm)	Density (% theor.)
Undoped Al_2O_3(II)						
No. 1	1500	0.5	1500	48	1.5	99.3
			1500	168	2.5	
			1600	48	10	
			1700	84	40	
No. 2	1600	1	1500	48	1*	99.4
Al_2O_3(II):Ti						
500 ppm Ti, No. 1	1600	0.5	1500	48	30	99.7
500 ppm Ti, No. 2	1450	0.5	1500	48	20	99.7
500 ppm Ti, No. 3	1400	0.5	1500	48	4	
			1600	48	15	
7000 ppm Ti	1550	1	1500	24	40	99.8
45 ppm Ti	1400	0.5	1500	48	4	99.6
20 ppm Ti	1400	0.5	1500	60	4	99.2
Al_2O_3(II):Fe						
3 wt% Fe	1500	0.5	1500	20	10	99.8
5000 ppm Fe	1500	0.5	1500	20	10	99.6
500 ppm Fe	1500	0.5	1500	20	10	99.7

*Irregular grains, some even 30 μm.

Table IV. Impurities in Al_2O_3 Found by Spectrochemical Analysis

Element	Amount detected (ppm) Al_2O_3(I)* Undoped	Undoped as-hot-pressed Al_2O_3(II)	As-hot-pressed Al_2O_3(II): 500 ppm Ti	Al_2O_3(II): 500 ppm Ti after electrical measurements	As-hot-pressed Al_2O_3(II): 3% Fe	As-hot-pressed Al_2O_3(II): 45 ppm Ti
Mg†	20	11	8.6	30	50	10
Fe‡	16	18	ND<10	32	30 000	< 10
Ca	43	4	3.3	73	10	3
Si	72	700	96	320	180	150
Mn	<20	<20	22	21	61	29
Cu	10.7	ND	2.2	0.59	4	< 1
Ti§	<10	<10	330	500	<10	49

*Ref 42. †1 ppm Mg=9.8×10^{16} cm^{-3}. ‡1 ppm Fe=4.27×10^{16} cm^{-3}. §1 ppm Ti=4.98×10^{16} cm^{-3}. ND=not detected.

donor. Since relatively small errors in absolute values can give rise to appreciable errors in the activation energies, absolute values of parameters calculated from the various effects, as well as activation energies, will be compared.

II. Experimental Procedure

(1) Sample Preparation

Alumina powder was made from aluminum isopropoxide $Al(OC_3H_7)_3$, purified by distillation in a vacuum of 20 mm Hg. The distilled fraction was 80%.

The purified liquid was poured into deionized water and stirred to form a gel of aluminum hydroxide. After drying and crushing, the hydroxide was decomposed in air at 850°C. Cylindrical samples (1.84 cm in diam. by 1.5 cm high) were made by hot-pressing in vacuum in a graphite die under a pressure of 55 MN/m^2 at 1400° to 1600°C. After hot-pressing, no black coloration was observed as it was in the material of Ref. 42 (Al_2O_3(I)), indicating the absence of transition elements in the new material, which will be labeled Al_2O_3(II).

For preparation of samples doped with Ti, the required amount of Ti isopropylate was mixed with Al isopropylate before precipitation; for Al_2O_3:Fe, iron sulfate was added to deionized water before pouring into aluminum isopropylate.

The large samples were sectioned into smaller ones for the measurements; rectangular blocks (6 by 3 by 3 mm) for the creep measurements and cylindrical plates (12 mm in diam. by 1 to 2 mm high) for the electrical measurements. The samples were annealed for two to seven days at 1500°C in air to stabilize the microstructure. Grain size (by the intercept method) and density (by pycnometry) were determined as described in Ref. 42.

The grain size d of the samples was increased by sintering the hot-pressed samples or varied by varying the temperature and/or time of hot-pressing. Table III shows densities and grain sizes of the various samples and the methods used to arrive at them. In accordance with findings by Arias[44] and Harmer *et al.*,[45] Ti is seen to promote grain growth. Inhomogeneous grain growth occurring in our samples may be due to inhomogeneity of the Ti concentration.[46]

Table IV gives concentrations of impurities and dopants as determined by semiquantitative spectrographic analysis. The results for undoped Al_2O_3 made from sulfate, Al_2O_3(I),[42] are shown for comparison. At the higher dopant concentrations, second-phase formation is to be expected and has in fact been observed. In some cases the concentrations in the samples after hot-pressing and those

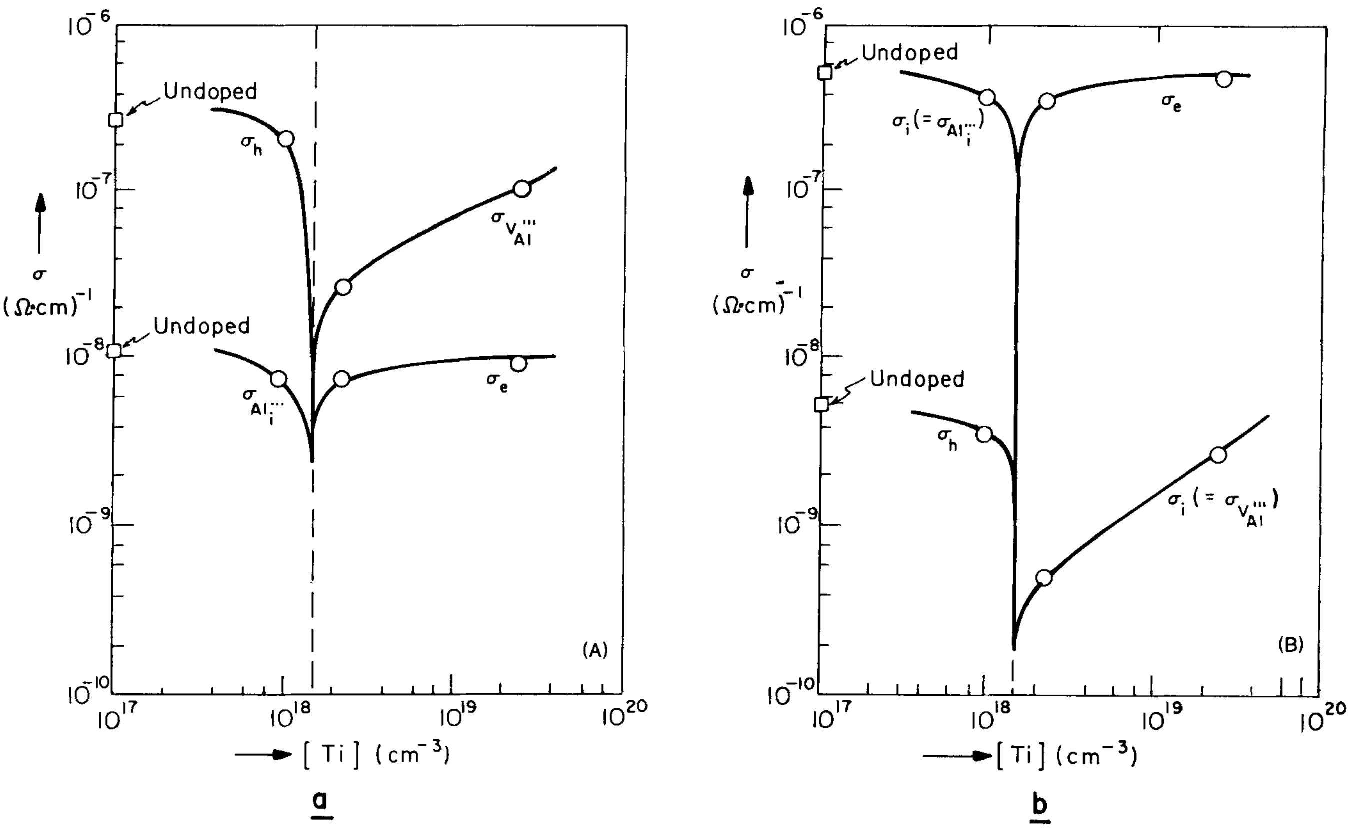

Fig. 1. Conductivity at 1500°C for Ti-doped $Al_2O_3(II)$ at p_{O_2}'s of (*a*) 10^5 and (*b*) 10^{-4} Pa.

after a prolonged anneal at high temperatures used to increase grain size are different; in particular, the increase in the Mg content may be significant.

(2) Electrical and Creep Measurements

Electrical conductivity of samples (σ) and the emf of oxygen concentration cells with the sample as electrolyte (E), were measured as a function of oxygen pressure, oxygen pressure gradients, and temperature, allowing long equilibration times to ensure maintenance of equilibrium with the atmosphere. A volume guard was used to eliminate gas-phase and surface conduction. Ionic transference numbers t_i were determined from emf E as a function of p_{O_2} by differentiating for p_{O_2}:

$$(t_i)p_{O_2,II}=[(4F/RT)\partial E/\partial \ln p_{O_2,II}]p_{O_2,I} \qquad (1)$$

Here F is the Faraday, R the gas constant, T the absolute temperature, and $p_{O_2,I}$ and $p_{O_2,II}$ the oxygen pressures at the two contacts. Partial ionic and electronic conductivities σ_i and σ_{el} were calculated from $\sigma_i=\sigma t_i$ and $\sigma_{el}=\sigma(1-t_i)$.

Creep was measured under compression as a function of stress (s), oxygen pressure (p_{O_2}), and temperature. Stresses were kept to ≤ 50 MN/m^2 to remain in the range of diffusion control. For a detailed description of the methods of measurement and the experimental setup, see Ref. 42 and earlier references given there.

III. Experimental Results

(1) Conductivity

Isotherms of undoped $Al_2O_3(II)$ measured from 1400° to 1600°C reveal the presence of partial ionic and electronic conductivities, decreasing and increasing, respectively, with increasing oxygen pressure. Evidently the electronic conductivity is a hole conductivity, i.e. the material is acceptor-dominated, as was $Al_2O_3(I)$.[42] Temperature-dependence studies show a simple exponential variation for σ_h but plots of log σ_i vs T^{-1} are curved, indicating contributions by two mechanisms with different activation energies, $(\sigma_i)_{high}$ and $(\sigma_i)_{low}$, a behavior not shown by $Al_2O_3(I)$; σ_{low} is independent of p_{O_2}. Similar effects were found for σ_i in the doped samples. The occurrence of $(\sigma_i)_{low}$ appears to be linked to SiO_2 present in $Al_2O_3(II)$ at a concentration sufficient to cause a second phase of aluminosilicate. This effect is important for the conductivity of polycrystalline ceramics at medium temperatures and deserves further study but is not important in the present context. Doping with Fe leaves the samples acceptor-dominated. Doping by Ti decreases the effective acceptor concentration up to the point of equivalence; beyond that point the material becomes donor-dominated and both σ_i (at high p_{O_2}) and σ_e (at low p_{O_2}) increase with increasing Ti concentration up to 500 ppm Ti (Fig. 1). At higher concentrations, the material reverts to *p*-type, probably due to the presence of a second phase. Electron microscopy indeed shows the presence of a second phase in $Al_2O_3(II)$:7000 ppm Ti and, to a smaller extent, even in $Al_2O_3(II)$:500 ppm Ti. The transition from *p*- to *n*-type material occurs at $\approx 10^{18}$ cm^{-3} Ti, indicating that this is the concentration of uncompensated acceptors in the undoped material. Combination of the absolute value of σ_i of undoped $Al_2O_3(II)$ with the ionic mobility $\mu_i=2\times10^8$ exp(-457 kJ/mol, RT) cm^2/V^{-1} s^{-1}, as reported in Ref. 41, gives an acceptor concentration of 1.5×10^{18} cm^{-3}. The fact that the two values are almost equal indicates that the acceptor involved is a fixed-valence element, probably Mg. Typical values of activation energies for ionic and electronic conductivities, σ_i and $\sigma_{el}=\sigma_e$ or σ_h of various undoped and doped samples, taken from graphs given in Ref. 47, are assembled in Tables V and VI. Oxygen pressure exponents r of the partial conductivities in isotherms are assembled in Table VII. Partial conductivities are $\propto[Fe]^y$ with $y=0.67$ for σ_i and 0.33 for σ_h, in agreement with $y=$ 0.67 to 0.73 obtained from sintering[12] but different from the values $y=0.33$ for σ_i and 0.62 for σ_h found for $Al_2O_3(I)$.[42] The former values must be preferred. Grain-size dependencies of the partial conductivities in $Al_2O_3(II)$, undoped and doped with Ti, are shown

Table V. Activation Energies of Conductivity and Creep Rate (in kJ/mol) for Undoped and Doped Polycrystalline Al_2O_3 made from Sulfate (I) and Propoxide (II) (Equilibrium Values)*

Sample	Dopant ppm X	d (µm)	$\dot{\varepsilon}$ (s=20–37 MN/m²)		σ_i		σ_e	σ_h
			air	$p_{O_2}=10^{-4}$ N/m²	$(\sigma_i)_{high}$	$(\sigma_i)_{low}$		
Al_2O_3(I)		3	543	626	366			183
		10			327			221
		20	626					
		100	844					
Al_2O_3(II)		1			>433			>231
		2	626		491	106		385
		6	565					
		10			443	118		327
		40	667		433	115		260
Al_2O_3(I)	500 Fe	3	584	543	423	106		298
		10			375			280
	5000 Fe	10	459	396	356			
	80 Ti	6			288		255	
Al_2O_3(II)	500 Fe	10			356	38		385
	5000 Fe	10			490	87		414
	30 000 Fe	10			481	67		452
	20 Ti	4			433	58		375
	45 Ti	4			490	58	606	
	500 Ti	4	459	459	481	58	597	
		20			337	48	558	
		30	418	543				
		40			481	58	587	298
	7000 Ti	25	625	584				
		40			356			
		100	584	584				

*In comparing activation energies of conductivity and creep, one should compare $H(\dot{\varepsilon})$ with $H(\sigma)+k\bar{T}\simeq H(\sigma)+15$ kJ/mol.

Table VI. Absolute Values of Partial Conductivities at 1600°C

Sample	Grain size (µm)	Absolute value ($\Omega^{-1}\cdot cm^{-1}$)		
		$(\sigma_i)_{high}$	$(\sigma_i)_{low}$	σ_e or σ_h
Al_2O_3(II)	1.5	3×10^{-6}	6×10^{-7}	$7\times10^{-6}(h^{\cdot})$
Al_2O_3(II):3 wt% Fe	10	1.5×10^{-5}	2×10^{-7}	$4.3\times10^{-6}(h^{\cdot})$
Al_2O_3(II):500 ppm Ti	40	2.5×10^{-6}	1.5×10^{-7}	$3\times10^{-6}(e')$

Table VII. Oxygen Pressure Exponents for Electronic and Ionic Conductivity and Creep Rate of Polycrystalline Al_2O_3 Samples

Sample	Oxygen pressure exponent, r			
	σ_h	σ_e	σ_i	ε
		Acceptor-dominated		
Undoped Al_2O_3(I)	0.22		0	
Al_2O_3(I):500 ppm Fe	.14		0	
Al_2O_3(I):5000 ppm Fe	.20		−0.1	−0.03
Undoped Al_2O_3(II)	.17		−0.2–0.24	−0.02
Al_2O_3(II):3 wt% Fe	.14		−0.14	−0.07
		Donor-dominated		
Al_2O_3(I):80 ppm Ti		−0.14	0.14	
Al_2O_3(II):500 ppm Ti		−0.18	0.17	0.015–0.03

in Figs. 2 and 3. The ionic conductivity is seen to increase slightly with grain size for undoped material, becoming constant at $d>10$ µm, a behavior similar to that found for Al_2O_3(I)[42]; σ_h of Al_2O_3(II) is independent of grain size, whereas that of Al_2O_3(I) decreased with increasing grain size up to $d=10$ µm.[42] The difference may be due to the presence in Al_2O_3(II) of a second phase of aluminosilicate, mentioned earlier in reference to $(\sigma_i)_{low}$. For Al_2O_3(II):500 ppm Ti, σ_i is practically independent of d, σ_e decreasing. Thus there appears to be a preference for grain-boundary conduction for electronic defects in some cases but grain boundaries either hinder ion migration or are indifferent.

(2) Creep

Creep rate follows a law

$$\dot{\varepsilon} \propto s^n d^{-m} p_{O_2}{}^r \exp(-H/RT) \quad (2)$$

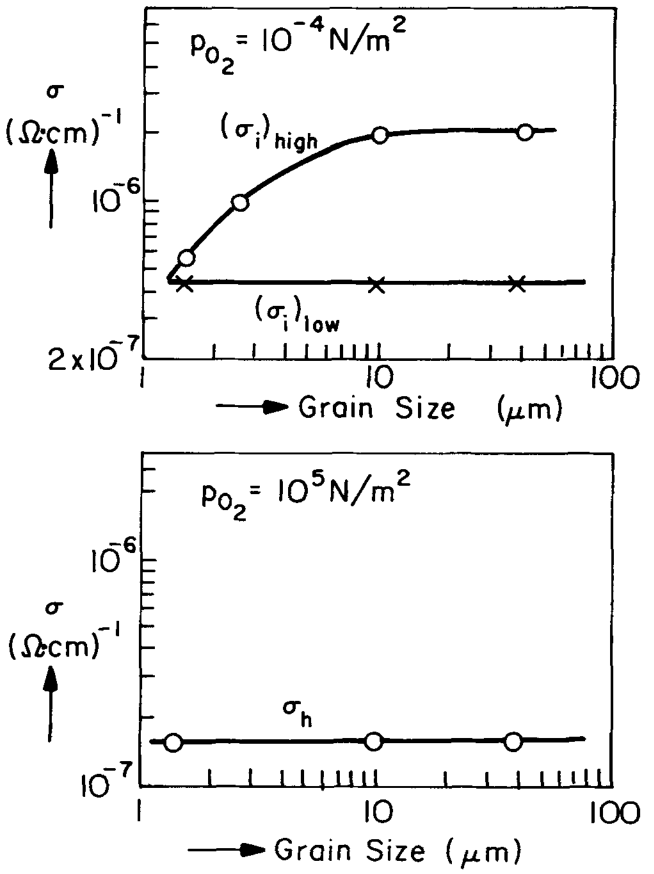

Fig. 2. Grain-size dependence of $(\sigma_i)_{high}$ and $(\sigma_i)_{low}$ at $p_{O_2}=10^{-4}$ Pa and of σ_h at $p_{O_2}=10^5$ Pa for undoped Al_2O_3(II) at 1500°C.

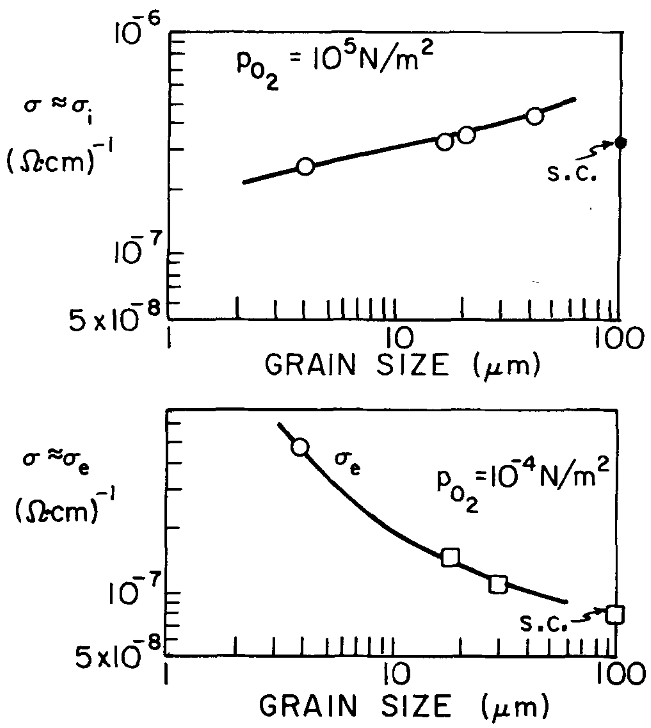

Fig. 3. Grain-size dependence of σ_i and σ_e for Al_2O_3(II):500 ppm Ti at 1500°C.

where s is stress, d grain size, H an activation enthalpy, and n, m, and r numerical constants. Values of H, r, and n obtained from graphs given in Ref. 48 are given in Tables V, VII, and VIII. At 1500°C, $s=30$ MN/m^2, and $p_{O_2}=2\times10^4$ Pa, grain-size exponents m have the value 2 for Al_2O_3(II), undoped, and doped with 500 ppm Ti, with $d=4$ to 40 μm; $m=3$ for Al_2O_3(II):7000 ppm Ti with $d=20$ to 100 μm. Typical absolute values of $\dot{\epsilon}$ at 1500°C, $p_{O_2}=2\times10^4$ Pa, and $s=30$ MN/m^2 are 5×10^{-3} (undoped, $d=6$ μm), 10^{-2} (500 ppm Ti, $d=4$ μm), and 1.4×10^{-2} (7000 ppm Ti, $d=25$ μm), all in h^{-1}. The values of the stress exponents $n=1.2$ to 1.3 indicate diffusion control with some contribution by either grain-boundary sliding, effects of dislocations near the grain boundaries, or creation and/or annihilation of point defects as a result of the applied stress. The grain-size exponent $m=2$ indicates bulk diffusion control (Nabarro-Herring mechanism). The value $m=3$ for Al_2O_3(II):7000 ppm Ti must be attributed to the presence of $TiAl_2O_5$ second-phase particles of a few micrometers at the grain boundaries,[49] the phase also held responsible for the anomalous p-type conductivity.

Our results differ from those reported by Cannon *et al.*[50] for fine-grained undoped and Mg-doped hot-pressed Al_2O_3 with $d=1$ to 15 μm and density 99.2 to 99.8; they found $n=1.47$ to 1.54 and $m=2.7$ to 2.9 and interpreted the results through a mixture of Al grain-boundary diffusion control (Coble creep, $n=1$, $m=3$) and interface control ($n=2$, $m=1$). The difference is no doubt due to the difference in grain size.

IV. Discussion

The ionic conductivity of undoped Al_2O_3(I)[42] and $(\sigma_i)_{high}$ of undoped Al_2O_3(II) increase with increasing grain size. Al_2O_3(I):Fe and Al_2O_3(II):Ti have σ_i independent of d. These facts prove that in neither acceptor- nor donor-dominated materials is there preferred ionic conduction along grain boundaries; grain boundaries hinder rather than help ionic conductivity. Increased migration of oxygen along grain boundaries, indicated by the increase of oxygen self-diffusion with decreasing grain size, reported by Oishi and Kingery,[2] and the decrease in the rate of chemical self-diffusion with increasing grain size in Al_2O_3:Ti and Al_2O_3:Fe[51] must therefore involve neutral species. For a constant concentration of oxidizable species, the rate of diffusion was found to be proportional to $p_{O_2}{}^r$ with $r={}^1/_2$ for Fe and $r={}^1/_3$ for Ti, the former value being equal to that expected for $O_i^{\times}$.[51]

Let us now see whether it is possible to find a defect model accounting for the following experimental facts:

(*a*) $(D_O)_{bulk} \ll (D_O)_{gb} \leq (D_{Al})_{bulk} = (D_{Al})_{gb}$ (Fig. 4) and similar inequalities for the corresponding conductivities with the exception of $(\sigma_O)_{gb}$, gb indicating grain boundary.

(*b*) Fast oxygen diffusion along grain boundaries by a neutral species, with bulk diffusion limiting creep at small grain sizes

(*c*) Oxygen pressure dependence of σ_i and σ_h and $\dot{\epsilon}$ as given in Table VII, in particular the difference between that of σ_i and $\dot{\epsilon}$

(*d*) Iron concentration dependence of σ_i and σ_h

Table VIII. Stress Exponents *n*

Sample	T (°C)	d (μm)	s(MN/m^2)	p_{O_2}(Pa)	Stress exp. n
Undoped Al_2O_3(II)	1450	2	5–50	2×10^4	1.3
Al_2O_3(II):500 ppm Ti	1500	30	7–40	2×10^4	1.25
Al_2O_3(II):7000 ppm Ti	1415	25	5–30	1	1.3

(*e*) Activation energies of creep and conductivity as observed (Table V)

(*f*) Variation of grain-size exponent of creep with increasing Fe content from 2 to >2[52]

(*g*) Increase of $(D_O)_{gb}$ by doping with iron[52]

In seeking for a model it should be kept in mind that any of these "facts" may be in error.

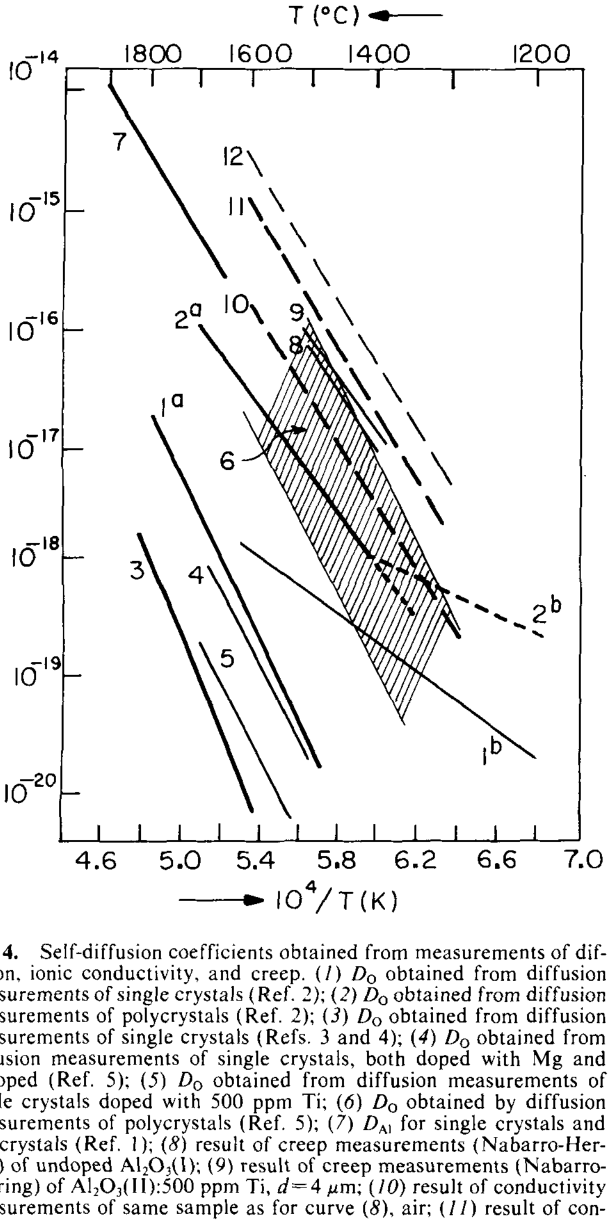

Fig. 4. Self-diffusion coefficients obtained from measurements of diffusion, ionic conductivity, and creep. (*1*) D_O obtained from diffusion measurements of single crystals (Ref. 2); (*2*) D_O obtained from diffusion measurements of polycrystals (Ref. 2); (*3*) D_O obtained from diffusion measurements of single crystals (Refs. 3 and 4); (*4*) D_O obtained from diffusion measurements of single crystals, both doped with Mg and undoped (Ref. 5); (*5*) D_O obtained from diffusion measurements of single crystals doped with 500 ppm Ti; (*6*) D_O obtained by diffusion measurements of polycrystals (Ref. 5); (*7*) D_{Al} for single crystals and polycrystals (Ref. 1); (*8*) result of creep measurements (Nabarro-Herring) of undoped Al_2O_3(I); (*9*) result of creep measurements (Nabarro-Herring) of Al_2O_3(II):500 ppm Ti, $d=4$ μm; (*10*) result of conductivity measurements of same sample as for curve (*8*), air; (*11*) result of conductivity measurements of Al_2O_3(II), $d=1.5$ μm, $p_{O_2}=10^{-4}$ Pa; (*12*) result of conductivity measurements of Al_2O_3(II):3 wt% Fe, $d=10$ μm, $p_{O_2}=10^{-4}$ Pa (present work).

In Ref. 42, the small activation energy of 241 kJ/mol observed for some oxygen diffusion processes (1*b* and 2*b* of Fig. 4) and the correspondence of this activation energy with that calculated for the mobility of $V_O^{\cdot\cdot}$ by Dienes *et al.*[53] were the basis of the assumption that $(D_O)_b$ could be $>D_{Al}$. However, the low activation energy process has been shown to be due to diffusion of oxygen along dislocations or subgrain boundaries[4,5]; for bulk diffusion $D_{Al}>>D_O$. Then the ionic conductivity of acceptor-dominated Al_2O_3 must be attributed to $\mathrm{Al}_i^{\cdot\cdot\cdot}$ and that of the donor-dominated Al_2O_3 to V_{Al}'''. Although it is likely that these species also dominate the neutrality condition, this is not necessarily so; in acceptor-doped material $V_O^{\cdot\cdot}$ may dominate the neutrality, but still $D_{Al}>D_O$ if the mobilities satisfy $\mu(\mathrm{Al})>>\mu(\mathrm{O})$. Table IX shows the exponents s and r for the concentrations of $V_O^{\cdot\cdot}$, $\mathrm{Al}_i^{\cdot\cdot\cdot}$, V_{Al}''', O_i'', $h^{\cdot}$, and e' in $[j]\propto[\mathrm{dopant}]^s p_{O_2}{}^r$ calculated on this basis for acceptor- and donor-doped Al_2O_3 with either the ionized or the neutral dopant species dominant; O_i'' is usually neglected because of the extremely large energy of formation expected for this species[53] but, in view of recent experimental results,[54] neglect of O_i'' may not be justified. The values of Table IX must be compared with the experimental values of r given in Table VII and the reported values of s.

The p_{O_2} exponents r for σ_h of undoped Al_2O_3(I) and (II) of 0.22 and 0.17 are not too different from the value 0.25 expected for Al_2O_3:Mg with $[\mathrm{Mg_{Al}}']\approx[\mathrm{Mg_{Al}}]_{total}$=constant; the values $r=0$ found for σ_i of undoped Al_2O_3(I) is just the value expected for Al_2O_3:Mg. The values $r=0.14$ to 0.20 observed for σ_h in Al_2O_3:Fe with $[\mathrm{Fe_{Al}}^{\times}]\approx[\mathrm{Fe}]_{total}$ are in reasonable agreement with those expected: 0.17 and 0.188 for the $V_O^{\cdot\cdot}$ and $\mathrm{Al}_i^{\cdot\cdot\cdot}$ models, respectively. The values 0 to 0.14 observed for σ_h in Al_2O_3:Fe containing considerable amounts of Mg are much smaller then the values $r=0.25$ and 0.188 expected for the $V_O^{\cdot\cdot}$ and $\mathrm{Al}_i^{\cdot\cdot\cdot}$ models, respectively. This difference could be explained if both Fe and Mg contribute in the neutrality condition:

$$2[V_O^{\cdot\cdot}] \text{ or } 3\,[\mathrm{Al}_i^{\cdot\cdot\cdot}]\approx[\mathrm{Mg_{Al}}']+[\mathrm{Fe_{Al}}'] \qquad (3)$$

In this case the expected values of r for σ_i are smaller than the values presented in Table IX. However, it would increase the value of r expected for σ_h to approximately 0.2.

The experimental values of the dopant concentration exponent s for Al_2O_3:Fe differ markedly for Al_2O_3(I) and Al_2O_3(II) but both indicate an increase of σ_i and σ_h with increasing iron concentration, showing that the Fe cannot be neglected relative to the Mg impurity. The best value for σ_i, $s=0.66$, fits almost exactly the model dominated by $[A]=2[V_O^{\cdot\cdot}]$, with $[A]_{total}\approx[A^{\times}]$. However, since Mg is present and tends to decrease s, the model with $[A]\simeq3[\mathrm{Al}_i^{\cdot\cdot\cdot}]$ with $s=1$ cannot be excluded and should in fact be preferred.

In the donor-dominated samples, ionic conduction should be limited by $[V_{Al}''']$; the experimental r values (0.14 and 0.17) are close to the value 0.188 expected for a model with $[\mathrm{Ti_{Al}}^{\times}]\approx[\mathrm{Ti}]_{total}$ and $[\mathrm{Ti_{Al}}^{\cdot}]\approx3[V_{Al}''']$; the value expected for the O_i'' model is 0.25. The r values of σ_e fit the V_{Al}''' and O_i'' models equally well. In view of the difference in the type of dominant defects, $\mathrm{Al}_i^{\cdot\cdot\cdot}$ for Al_2O_3:Fe and V_{Al}''' for Al_2O_3:Ti, the similarity in the absolute values of σ in acceptor- and donor-doped material must be fortuitous.

Let us now consider creep. If there is fast grain-boundary dif-

Table IX. Values of s and r in $[j]\,\alpha p_{O_2}{}^r\,[\mathrm{dopant}]^s$ for Various Species for Different Approximations of Neutrality Condition for Acceptor- and Donor-Doped Al_2O_3

	$[A']\approx[V_O\ ]$				$[A']\approx3[\mathrm{Al}_i\ ]$				$[D']\approx3[V_{Al}\ ]$				$[D']=2[O_i'']$			
	$[A']=[A]_{total}$		$[A^{\times}]=[A]_{total}$		$[A']=[A]_{total}$		$[A^{\times}=[A]_{total}$		$[D]=[D]_{total}$		$[D^{\times}]=[D]_{total}$		$[D\ ]=[D]_{total}$		$[D^{\times}]=[D]_{total}$	
Species	s	r	s	r	s	r	s	r	s	r	s	r	s	r	s	r
$V_O^{\cdot\cdot}$	1	0	0.67	−0.17	0.67	0	0.5	−0.125	−0.67	0	−0.5	−0.125	−1	0	−0.67	−0.167
$\mathrm{Al}_i^{\cdot\cdot\cdot}$	1.5	0	1	−0.25	1	0	0.75	−0.188	−1	0	−0.75	−0.188	−1.5	0	−1	−0.25
$h^{\cdot}$	0.5	0.25	0.33	0.17	0.33	0.25	0.25	0.188	−0.33	0.25	−0.25	0.188	−0.5	0.25	−0.33	0.167
V_{Al}'''	−1.5	0	−1	0.25	−1	0	−0.75	0.188	1	0	0.75	0.188	1.5	0	1	0.25
O_i''	−1	0	−0.67	0.17	−0.67	0	−0.5	0.125	0.67	0	0.5	0.125	1	0	0.67	0.167
e'	−0.5	−0.25	−0.33	−0.17	−0.33	−0.25	−0.25	−0.188	0.33	−0.25	0.25	−0.188	0.5	−0.25	0.33	−0.167

fusion of oxygen, creep must involve bulk diffusion of Al. However, since our experiments indicate that the diffusing oxygen is neutral, the Al bulk diffusion must be ambipolar, involving both ionic and electronic defects, i.e. $\mathrm{Al}_i^{\cdot\cdot\cdot}$ and $h^{\cdot}$ in acceptor-dominated samples, V_{Al}''', and e' in donor-dominated samples.

As outlined in Ref. 42, in such cases the rate is determined by the species with the smaller concentration × mobility product. Our experiments show that in acceptor-dominated samples $\sigma_h > \sigma_i$ at high p_{O_2} but $\sigma_h < \sigma_i$ at low p_{O_2} Thus there should be a change of rate-limiting species from $\mathrm{Al}_i^{\cdot\cdot\cdot}$ at high to $h^{\cdot}$ at low p_{O_2}. Donor-doped samples show the opposite conductivity behavior, with $\sigma_e > \sigma_i$ at low p_{O_2}, requiring a change of rate-limiting species from e' at high to V_{Al}''' at low p_{O_2}. Such a change should affect both the activation energy and the oxygen pressure dependence of creep rate.

In the acceptor-dominated samples, the oxygen pressure dependence of ε of Al_2O_3(I) with or without Fe is close to that of σ_i and different from that of σ_h (see Table VII). As seen in Table V, the activation energy of creep is significantly larger than that of σ_i (and much larger than that of σ_h), in particular for Al_2O_3(I), but also for Al_2O_3(II) where activation energies of ionic conduction as large as 491 kJ/mol (5.1 eV) have been observed, compared with 577 kJ/mol (6 eV) for creep. This difference suggests limitation of σ_i and $\dot{\varepsilon}$ by different species, one by Al and the other by O. The activation energies of creep do not change appreciably with a change in p_{O_2} (see Table V), so there is no indication of limitation of creep by holes at low p_{O_2}. For Al_2O_3:Ti, the activation energies of σ_i, σ_e, and $\dot{\varepsilon}$ are approximately equal, indicating that σ_i and ε may be limited by the same ionic species (V_{Al}''') but leaving open the possibility of limitation of creep by electrons. For σ_i as well as $\dot{\varepsilon}$ we expect a weak p_{O_2} dependence for undoped (=Mg-doped) material (Table IX, $[A] \approx [A']$) but a marked p_{O_2} dependence for Al_2O_3:Fe and Al_2O_3:Ti (Table IX, $[A] \approx [A^{\times}]$ or $[D] \approx [D^{\times}]$). This is in fact observed for σ_i but not for $\dot{\varepsilon}$ which is almost independent of p_{O_2}. A p_{O_2} dependence for Al_2O_3:Ti with $r=0.1$, weaker than that expected on the basis of defect models ($r=0.188$ or 0.25) was also found by Hollenberg and Gordon[20] but was not explained. The effect can have various causes: ambipolar diffusion, precipitation of a second phase, or formation of defects by plastic deformation in concentrations larger than those resulting from doping. Ambipolar diffusion with rate limitation by V_{Al}''' at low and by e' at high p_{O_2} gives a considerable reduction in p_{O_2} dependence because these species have opposite values of r. However, calculation of the effective self-diffusion coefficient from

$$(D_{\mathrm{Al}})_b = \frac{3D(V_{\mathrm{Al}}''')D(e')[V_{\mathrm{Al}}'''][e']}{9D(V_{\mathrm{Al}}''')[V_{\mathrm{Al}}''']+D(e')[e']} \qquad (4)$$

with r values of + and -0.188 for σ_i and σ_e and $\sigma_i = 10\,\sigma_e$ at $p_{O_2} = 10^5$ N/m^2 gives a p_{O_2} dependence of $(D_{\mathrm{Al}})_b$ with a maximum at intermediate p_{O_2}, with values at the maximum that are four times larger than at high and low p_{O_2}. Such a maximum is not observed. Formation of a second phase to an extent increasing with increasing p_{O_2} is to be expected and should affect creep rate. However, it should affect σ_i in the same way, which is not observed, σ_i having a stronger p_{O_2} dependence than $\dot{\varepsilon}$. This leaves defect formation during deformation as a possible cause. However, this effect is generally believed to be appreciable only at stresses much higher than the ones used in our experiments. Repetition of the experiments with purer material, using lower stresses, and with different doping concentration, should indicate whether any of the suggested explanations are valid.

Let us now consider the absolute values. Figure 4 shows values of the self-diffusion coefficient $D_{\mathrm{self}} = [j]D_j$ as determined by tracer diffusion of Al and O, and as calculated from conductivity and creep, the former using the Nernst-Einstein relation, $D = \sigma_i kT/Nz_i^2q^2$ (with N the number of Al_2O_3 molecules cm^{-3}, z_i the defect charge, and q the electron charge), the latter calculated on the basis of the Nabarro-Herring theory, $\dot{\varepsilon} = 13.3\, D_b \Omega s/kTd^2$ (with Ω the molar volume of Al_2O_3, 4.2×10^{-23} cm$^3 = N^{-1}$, and s the stress).

It is seen that the values calculated from creep (curves 8 and 9) and conductivity (curves 10 to 12) are close together, being almost the same for undoped (=Mg-doped) material (curves 8, 10, and 11) and for material doped with Fe or Ti (curves 9 and 12). All values are close to those for self-diffusion of Al (curve 7) but much higher than those for bulk self-diffusion of O in either donor- or acceptor-dominated Al_2O_3 (curves 1*a*, 3, 4, and 5). This result strongly suggests that creep and conductivity are both limited by Al with $\mathrm{Al}_i^{\cdot\cdot\cdot}$ and V_{Al}''' the native defects involved in acceptor- and donor-dominated material.

Still to be explained is the lack of creep limitation by σ_h for Al_2O_3:Fe at low p_{O_2} and the increase of oxygen grain-boundary diffusion by doping with iron.[52] Both effects would be expected should grain-boundary diffusion of oxygen involve charged species. If the assumption of grain-boundary diffusion by neutral $\mathrm{O}_i^{\times}$ is maintained, the increase with doping could be due to pore formation.[55]

Finally, it is necessary to account for the high activation energy (750 to 844 kJ/mol) found for large grain samples in which creep is limited by dislocation climb.[19,20,42] This effect can be attributed either to oxygen bulk diffusion (observed activation energies 635,[2] 741,[4] and 616 kJ/mol[5]) or to the complexities of the climb process itself.[56-58]

V. Summary

Measurements of dc conductivity, ionic and electronic transference numbers, and creep were performed for hot-pressed polycrystalline Al_2O_3, of various grain sizes, made from aluminum propoxide (Al_2O_3(II)), undoped and doped with Fe or Ti. The undoped material still contains 1.5×10^{18} cm^{-3} fixed-valency acceptors (Mg). Because of these impurities, the p_{O_2} dependence of conductivity of samples doped with Fe or Ti is smaller than expected for samples dominated by these dopants alone. Conductivity with a low activation energy found at low temperatures is attributed to a second phase. Fast ionic diffusion along grain boundaries is absent in donor- as well as acceptor-doped samples. Therefore, fast diffusion along grain boundaries must involve neutral species. Absolute values of self-diffusion coefficients calculated from conductivity and creep indicate that both effects are limited by Al. Yet some effects remain unexplained.

References

[1] A. E. Paladino and W. D. Kingery, "Aluminum Ion Diffusion in Aluminum Oxide," *J. Chem. Phys.*, **37** [5] 957–62 (1962).

[2] Y. Oishi and W. D. Kingery, "Self-Diffusion of Oxygen in Single Crystal and Polycrystalline Aluminum Oxide," *ibid.*, **33** [2] 480–86 (1960).

[3] D. J. Reed and B. J. Wuensch, "Ion Probe Measurement of Oxygen Self-Diffusion in Single Crystalline Al_2O_3," *J. Am. Ceram. Soc.*, **63** [1–2] 88–92 (1980).

[4] D. J. Reed and B. J. Wuensch, "Ion Probe Measurement of Oxygen Self-Diffusion in Al_2O_3," *Am. Ceram Soc. Bull.*, **56** [3] 298 (1977).

[5] K. P. R. Reddy, "Oxygen Diffusion in Close Packed Oxides"; Ph.D. Thesis, Case Western Reserve University, Cleveland, Ohio, 1979.

[6] G. C. Kuczynski, L. Abernethy, and J. Allan, pp. 163–72 in Kinetics of High-Temperature Processes. Edited by W. D. Kingery. M.I.T. Press, Cambridge, Mass., 1959.

[7] R. L. Coble, "Initial Sintering of Alumina and Hematite," *J. Am. Ceram. Soc.*, **41** [2] 55–62 (1958).

[8] C. A. Bruch, "Sintering Kinetics for the High-Density Alumina Process," *Am. Ceram. Soc. Bull.*, **41** [12] 799–806 (1962).

[9] D. L. Johnson and I. B. Cutler, "Diffusion Sintering," *J. Am. Ceram. Soc.*, **46** [11] 541–50 (1963).

[10] R. D. Bagley, "Effects of Impurities on the Sintering of Alumina"; Ph.D. Thesis, University of Utah, Salt Lake City, June 1964.

[11] R. D. Bagley, I. B. Cutler, and D. L. Johnson, "Effects of TiO_2 on Initial Sintering of Al_2O_3," *J. Am. Ceram. Soc.*, **53** [3] 136–41 (1970).

[12] W. Raja Rao and I. B. Cutler, "Effect of Iron Oxide on the Sintering Kinetics of Al_2O_3," *ibid.*, **56** [11] 588–93 (1973).

[13] R. L. Coble, "Sintering Crystalline Solids: II," *J. Appl. Phys.*, **32** [5] 793–99 (1961).

[14] D. A. Krohn, P. A. Urick, D. P. H. Hasselman, and T. G. Langdon, "Evidence for Coble Creep in the Relaxation of Surface-Compressive Stresses in Tempered Polycrystalline Aluminum Oxide," *ibid*, **45** [9] 3729–31 (1974).

[15] R. C. Folweiler, "Creep Behavior of Pore-Free Polycrystalline Alumina,' *ibid.*, **32** [5] 773–78 (1961).

[16] S. I. Warshaw and F. H. Norton, "Deformation Behavior of Polycrystalline Aluminum Oxide," *J. Am. Ceram. Soc.*, **45** [10] 479–86 (1962).

[17] I. I. Vishnevskii, E. I. Akselrod, and N. D. Talyanskaya, "Diffusion Creep of Corundum," *Sov. Phys. Solid State*, **13** [11] 2910–11 (1972).

[18] R. Chang, "Creep of Al_2O_3 Single Crystals," *J. Appl. Phys.*, **31** [3] 484–87 (1960).

[19] E. I. Akselrod, I. I. Vishnevskii, E. R. Dobrovinskaya, and N. D. Talyanskaya, "High-Temperature Creep of Corundum Crystals in the Case of Pure Bending," *Sov. Phys. Dokl. (Engl. Transl.)*, **18** [11] 683–85 (1974).

[20] G. W. Hollenberg and R. S. Gordon, "Effect of Oxygen Partial Pressure on Creep of Polycrystalline Al_2O_3 Doped with Cr, Fe, Ti," *J. Am. Ceram. Soc.*, **56** [3] 111–72 (1973).

[21] T. Maruyama and W. Komatsu, "Surface Diffusion of Single Crystal Al_2O_3 by the Scratch Smoothing Method," *ibid.*, **58** [7–8] 338–39 (1975).

[22] P. J. Harrop and R. W. Creamer, "High-Temperature Electrical Conductivity of Single Crystal Alumina," *Br. J. Appl. Phys.*, **14** [6] 335–39 (1963).

[23] O. T. Oezkan and A. J Moulson, "Electrical Conductivity in Single Crystal and Polycrystalline Aluminum Oxide," *J. Phys. D*, **3** [6] 983–86 (1970)

[24] R. J. Brook, J. Yee, and F. A. Kroeger, "Electrochemical Cells and Electrical Conduction of Pure and Doped Al_2O_3," *J. Am. Ceram. Soc.*, **54** [9] 444–51 (1971).

[25] J. Yee and F. A. Kroeger, "Measurements of Electromotive Force in Al_2O_3—Pitfalls and Results," *ibid.*, **56** [4] 189–91 (1973).

[26] J J Mills, "Non-Stoichiometric Defects in Sapphire," *J. Phys. Chem. Solids*, **31** [11] 2577–79 (1970).

[27] G. M. Stulova and Yu. K. Shalabutov, "Investigation of the Electrical and Optical Properties of Synthetic Sapphire at High Temperatures," *Sov. Phys. Semicond*, **1** [8] 996–97 (1968).

[28] H. M. Kizilyalli and P R. Mason, "D.C. and A.C. Electrical Conduction in Single Crystal Alumina," *Phys. Status Solidi A*, **36** [2] 499–508 (1976).

[29] (*a*) W. J. Lackey, Jr., "Effect of Temperature on Electrical Conductivity and Transport Mechanism in Sapphire," *Mater. Sci. Res.*, **5,** 489–502 (1971)

(*b*) W. J Lackey, Jr., "Electronic and Ionic Conductivity in Alumina," *Univ. Microfilms Int.*, (Ann Arbor, Mich.) *Order No.* 71–10 256.

[30] K. Kitazawa and R L. Coble, "Electrical Conduction in Single Crystal and Polycrystalline Al_2O_3 at High Temperatures," *J. Am. Ceram. Soc.*, **57** [6] 245–50 (1974).

[31] J. L. Kemp and A. J Moulson, "The Effect of Iron Additions on the Electrical Properties of Alumina Ceramics," *Proc. Br. Ceram Soc.*, **18,** 53–64 (1970).

[32] H. P. R. Frederikse and W R. Hosler, "High-Temperature Electrical Conductivity Techniques," Rept. No. ARL 73–0156, Aerospace Research Lab (USAF), Wright Patterson Air Force Base, Ohio, 1973.

[33] N. M. Tallan and H. C. Graham, "Interfacial Polarization and Electrical Conductivity in Sapphire," *J. Am. Ceram. Soc.*, **48** [10] 512–16 (1965).

[34] D. W. Peters, L. Feinstein, and C. Peltzer, "High-Temperature Electrical Conductivity of Alumina," *J. Chem. Phys.*, **42** [7] 2345–46 (1965).

[35] V. I. Aleksandrov, V V. Osiko, and V. M. Tatarintsev, "Electrical Conductivity in Fused Aluminum Oxide," *Inorg Mater.*, **8** [5] 835–36 (1972).

[36] B. V. Dutt, J. P. Hurrell, and F. A. Kroeger, "High-Temperature Defect Structure of Cobalt-Doped α-Alumina," *J. Am. Ceram. Soc.*, **58** [9–10] 420–27 (1975).

[37] B. V. Dutt and F. A. Kroeger, "High-Temperature Defect Structure of Iron-Doped α-Alumina," *ibid.*, [11–12] 474–76 (1975) (Interpretation of experimental results of Ref. 38).

[38] J Pappis and W. D. Kingery, "Electrical Properties of Single Crystal and Polycrystalline Alumina at High Temperatures," *ibid.*, **44** [9] 459–64 (1961).

[39] S. K. Mohapatra and F. A. Kroeger, "Defect Structure of α-Al_2O_3 Doped with Magnesium," *ibid*, **60** [3-4] 141–48 (1977)

[40] S. K. Mohapatra and F. A. Kroeger, "The Defect Structure of α-Al_2O_3 Doped with Titanium," *ibid.*, [9-10] 381–87

[41] S. K. Mohapatra, S. Tiku, and F. A. Kroeger, "The Defect Structure of Unintentionally Doped α-Al_2O_3 Crystals," *ibid.*, **62** [1–2] 50–57 (1979).

[42] L. D. Hou, S. K. Tiku, H. A. Wang, and F. A. Kroeger, "Conductivity and Creep of Acceptor-Dominated Polycrystalline Al_2O_3," *J. Mater. Sci.*, **14** [8] 1877–89 (1979).

[43] S. K. Tiku and F. A. Kroeger, "Effect of Space Charge, Grain-Boundary Segregation, and Mobility Differences between Grain Boundary and Bulk on the Conductivity of Polycrystalline Al_2O_3," *J. Am. Ceram. Soc.*, **63** [3–4] 183–89 (1980).

[44] A Arias, "Effect of Inclusions on Grain Growth of Oxides," *ibid.*, **49** [11] 621–24 (1966).

[45] M. Harmer, E. W. Roberts, and R. J. Brook, "Rapid Sintering of Pure and Doped α-Al_2O_3," *Trans. Br. Ceram. Soc.*, **78** [1] 22–24 (1979).

[46] J. G. J. Peelen, "Alumina: Sintering and Optical Properties," Thesis, Technische Hogeschool, Eindhoven, The Netherlands, 1977.

[47] H. A. Wang, "High-Temperature Electrical Conductivity and Defect Structure of Undoped and Doped Polycrystalline Alumina," Thesis, University of Southern California, June 1980.

[48] L. D. Hou, "Creep and Defect Structure of Polycrystalline Alumina," Thesis, University of Southern California, June 1980.

[49] R. Raj and M. F. Ashby, "On Grain Boundary Sliding and Diffusional Creep," *Metall. Trans.*, **2** [4] 1113–27 (1971).

[50] R. M. Cannon, W. H. Rhodes, and A. H. Heuer, "Plastic Deformation of Fine-Grained Alumina (Al_2O_3):I," *J. Am. Ceram. Soc*, **63** [1–2] 46–52 (1980).

[51] H. A. Wang and F. A. Kroeger, "Chemical Diffusion in Polycrystalline Al_2O_3," *ibid.*, [11–12] 613–19.

[52] P. A. Lessing and R. S. Gordon, "Creep of Polycrystalline Alumina, Pure and Doped with Transition Metal Impurities," *J. Mater. Sci.*, **12** [11] 2291–2302 (1977).

[53] G. J. Dienes, D. O. Welch, C. R. Fischer, R. D. Hatcher, O. Lazareth, and M. Samberg, "Shell-Model Calculations of Some Point Defect Properties in α-Al_2O_3," *Phys. Rev. B*, **11** [8] 3060–70 (1975).

[54] D. S. Phillips, T. E. Mitchell, and A. H. Heuer, "Precipitation in Star Sapphire: III," *Philos. Mag.*, **42A** [3] 417–32 (1980).

[55] H. A. Wang and F. A. Kroeger, "Pore Formation During Oxidative Annealing of Al_2O_3:Fe and Slowing of Grain Growth by Precipitates and Pores," *J. Mater. Sci.*, **15** [8] 1978–86 (1980).

[56] B. Escaig, "Some New Problems Encountered in the Deformation of Oxides," *J. Phys. (Orsay, France)*, **33** [10] 919–27 (1972).

[57] C. Monty, "Point Defects in Oxides; Non-Stoichiometry and Transport of Material," *ibid.*, **39** [Suppl. No. 6][C2] 74–85 (1978).

[58] T. Bretheau, J. Castaing, J. Rabier, and P. Veyssiére, "Movement of Dislocations and Plasticity at High Temperatures in Binary and Ternary Oxides," *Adv. Phys.*, **28** [6] 835–1014 (1979); especially pp. 911ff.

Temperature/Composition Phase Diagram of the System Bi_2O_3-PbO

R. M. BIEFELD

Sandia Laboratories, Albuquerque, New Mexico 87185

S. S. WHITE*

Sandia Laboratories, Livermore, California 94550

The Bi_2O_3-PbO phase diagram was determined using differential thermal analysis and both room- and high-temperature X-ray powder diffraction. The phase diagram contains a single eutectic at 73 mol% PbO and 635°C. A body-centered cubic solid solution exists above ≈600°C within a composition range of 30 to 65 mol% PbO. The compounds α-Bi_2O_3, δ-Bi_2O_3, and γ-PbO (litharge) have wide solubility ranges. Four compounds, $6Bi_2O_3 \cdot PbO$, $3Bi_2O_3 \cdot 2PbO$, $4Bi_2O_3 \cdot 5PbO$, and $Bi_2O_3 \cdot 3PbO$, are formed in this system and the previously unreported X-ray diffraction patterns of the latter three compounds are reported. Diffraction patterns for some of these mixed oxides have been observed in ZnO-based varistors grown using Bi_2O_3 and PbO as sintering aids.

I. Introduction

The interest in the Bi_2O_3+PbO phase diagram arises because PbO and Bi_2O_3 are used as sintering aids for the preparation of ZnO high-field varistors. A varistor is a variable resistor in that its resistance decreases rapidly with increasing voltage above a certain threshold voltage.[1,2] Because this breakdown voltage is strongly dependent on grain size, it is important to limit the size of the ZnO grains for a high-field device. Since PbO and Bi_2O_3 form a low-melting eutectic, relatively low temperatures can be used in the preparation of ZnO varistors, and only limited grain growth takes place.[2] The definition of the liquidus temperatures in the system Bi_2O_3-PbO should be of aid in the preparation of varistors.

Varistors are usually prepared from a mixture of metal oxides such as ZnO, CoO, Bi_2O_3, and PbO. Although several theories have been proposed to explain the effects of certain oxides on the properties of varistors, their roles are not completely understood or characterized. While it is thought that Bi_2O_3 does not affect the electrical properties of the ZnO grains themselves, it has been postulated that Bi_2O_3 affects the electrical properties of the grain boundaries of varistors.[1-4] The existence of compounds and the formation of solid solutions in the system Bi_2O_3-PbO could affect the performance of the varistors. Although several determinations of the Bi_2O_3-PbO phase diagram are reported, none are complete, and the results are somewhat contradictory.[5-11] This investigation of the Bi_2O_3-PbO phase diagram was undertaken to determine what reactions and compounds exist in the system Bi_2O_3-PbO and the temperatures and compositions at which these reactions and compounds occur.

II. Experimental Procedure

The phase diagram of the system Bi_2O_3-PbO was examined by

Presented at the 82nd Annual Meeting, The American Ceramic Society, Chicago, Illinois, April 28, 1980 (Basic Science Division No 46–B–80). Received June 20, 1980; revised copy received September 9, 1980.

Supported by the U S Department of Energy under Contract No. DE AC04 76 DP00789.

*Member, the American Ceramic Society.